Forbidden oxygen in the Milky Way disk

Asma Sahli

Lund Observatory
Lund University

2017-EXA121

Degree project of 15 higher education credits
June 2017

Supervisor: Thomas Bensby

Lund Observatory
Box 43
SE-221 00 Lund
Sweden

July 19, 2017

Abstract

Oxygen is produced inside massive stars and dispersed into the interstellar medium mainly through type II supernovae explosions. This element, which is the third most abundant one in the Universe, plays an important role in tracing the Galactic chemical history and evolution.
This study aims at determining oxygen abundances from a sample of 714 F and G dwarf stars located in the solar neighborhood, from the oxygen forbidden line located at 6300Å, which is very weak and blended with a nickel line. This sample has been already used for a similar study (Bensby et al. 2014), but abundances were determined via the triplet oxygen lines found at 7774Å, which are strong but formed under Non-Local Thermodynamic Equilibrium (NLTE) conditions. However, these departures were corrected for with empirical methods. Therefore, the resulting oxygen abundances from the forbidden line were compared to those obtained from the triplets, to test the reliability of this indicator within the sample of 714 stars.

High-resolution spectra of these stars were obtained with high signal-to-noise, from observations conducted at some of the World's largest telescopes. Abundances for oxygen were calculated by spectral fitting of the observed and synthetic spectra using LTE model atmospheres obtained from MARCS (Gustafsson et al. 2008).
We find that the forbidden line was not a reliable indicator for determining oxygen abundances from the 714 stars sample, in comparison with the 7774Å.

Finally, to explain the reason behind the failure of the forbidden line, uncertainties and possible error sources were individually studied. Unfortunately, either the sample was not good enough to be used for this indicator, as it only gives reasonable results when used for the triplet lines, or the adapted routine for the analysis had been erroneous.

Populärvetenskaplig sammanfattning på svenska

Syre är det tredje vanligaste grund ämnet i rymden efter väte och helium. Det förekommer naturligt i tre stabila isotoper; nämligen ^{16}O, ^{17}O och ^{18}O. ^{16}O är den dominerande syreisotopen och den huvudsakliga produkten vid kärnbr änning av helium och neon. Dessa reaktioner kan ta mellan 3 och 10^6 år och sker vanligen i det inre omr ådet av massiva stj ärnor med exempelvis åtta gånger solens massa.

Syre anses vara ett viktigt spår ämne för vintergatan kemiska evolution då dess förekomst kan mätas på olika platser med hjälp av en mängd olika metoder. Detta kan i sin tur anv ändas för att best ämma den kemiska uppbyggnaden av gaser som återfinns i en stj ärnas atmosf är (Amarsi et al. 2016). Att best ämma förekomsten av syre på olika områden i vår galaxär alltså en mycket intressant uppgift då denna information kan hjälpa oss förstå stjärnpopulationens evolution och historia. Dessutom kan syreförekomsten hjälpa oss att bättre förstå tidsförloppet vid supernovor. Exempelvis har thin disk stjärnor med höga metalliciteter lågt syre och tros vara värd till fler supernovae av typ Ia, vilka bidrar till rymdmateria med få alpha-element (ex. O ,Mg, Si, S,Ca och Ti) och mycket järn. Till skillnad från dessa är thick disk stjärnor med låg metal- icitet rika på syre och tros därför vara värd till fler supernovae av typ II. Dessa producerar med alpha element och mindre järn. Vidare kan vi, med hjälp av bra mätningar av syref örekomst i metallfattiga kärnor, ge ett bättre estimat av dessas ålder. Denna typ av stjärnor tillhör thick disk regionen. En metod att analysera syreförekomsten i solarlika stjärnor är att undersöka spektralinjerna 7700 Å triplett som är starka och fria från överlapp från andra ämnen. 7700 Å triplett linjerna formas dock bara under extrema föruts ättningar som skiljer sig markant från den lokala thermodynamiska jämnvikten. En annan metod för att best ämma syref örekomst är att unders öka den förbjudna linjen vid 6300 Å som är svag och överlappar en del med en spektrallinje från nickel. Denna linjen formas under den lokala thermodynamiska jämnvikten och valdes att unders ökas i detta projekt på grund av denna viktiga egenskap. Det dataset som användes inneh åller 714 högkvalitativa stellarspektra fråan typ F och G stjärnor i vår omgivning. Denna data har använts tidigare för undersökning av syref örekomst men då inte med 6300 Å linjen (Bensby et al. 2014). Detta projektet ämnar undersöka trovärdigheten av 6300 Å linjen som indikator av syreförekomst för det ovanämnda dataset. Detta görs genom jämf örelse med resultat från 7700 Å tripplet linjerna. Syref örekomsten ber äknades genom spektralanpassning av det observerade och det syntetiska spektra. Det syntetiska spektrat producerades med hjälp av en mjukvara vid namn SME (spectroscopy made easy).

Contents

Chapter 1

Introduction

Oxygen is the third most abundant element in the Universe, after hydrogen and helium, and forms mainly inside massive stars during hydrostatic nucleo-synthesis of alpha particles (Bertran de Lis et al. 2015). When these stars explode as type II supernovae (SN II), the interstellar medium is enriched by the elements ejected by the star, and in particular, oxygen.

Oxygen is an important element for the study of galactic history and formation. For instance, by comparing the oxygen abundance to iron abundance, which is an element that is made in both SN II and SN Ia, it is possible to analyze many proprieties of a system of stars, such as its formation timescale and the star formation rate (McWilliam 1997).

Our galaxy, the Milky Way, is currently a unique galaxy in which stellar populations can be studied in detail. It is therefore essential to reveal the mystery behind their formation history and evolution, as this can also help understand proprieties of other galaxies in the Universe.

There exist several methods to determine oxygen abundances, for example the analysis of the triplet atomic oxygen spectral lines located at $7770 - 7774$Å. These lines are strong and not blended but are formed under Non-LTE conditions, and can give wrong results if not analyzed correctly (Amarsi et al. 2016). On the other hand, the 6300Å oxygen forbidden line is weak, often affected by telluric lines and contains a nickel blend. It also presents the enormous benefit of being formed under LTE conditions and gives very reliable oxygen abundances.

During this project, the study of oxygen abundances was based on the forbidden line, and were calculated via the spectral fitting of the observed and synthetic spectra. To check the reliability of this line, results were then compared to abundances obtained from the triplet lines from a previous study (Bensby et al. 2014). High-resolution observations were conducted in the World's largest telescopes to collect spectra for 714 F and G dwarf stars in the Solar neighborhood. The sample contains turn-off, subgiants and main-sequence stars, which have proprieties similar to those of our Sun, making their analysis easier than for other types. Spectra within this sample contain both the forbidden and triplet lines.

Chapter 2

Background

2.1 The Milky Way

Figure 2.1: Artist impression of the Milky Way Galaxy (Alothman 2016)

Our home galaxy, the Milky way, illustrated in figure 2.1, is a barred spiral galaxy that is estimated to host from 100 up to 400 billion stars. Estimates of its diameter ranges between 31-55 kpc across, and its age has been evaluated to be about 13 billion years. Our Sun is located at 8-8.5 kpc from the Galactic center. The stellar component of the Milky Way can be viewed as the assembly of four structural components; A bulge, a stellar halo, a thin and a thick disk, represented by figure 2.2. The main focus of this project will be targeted towards the thin and thick disks.

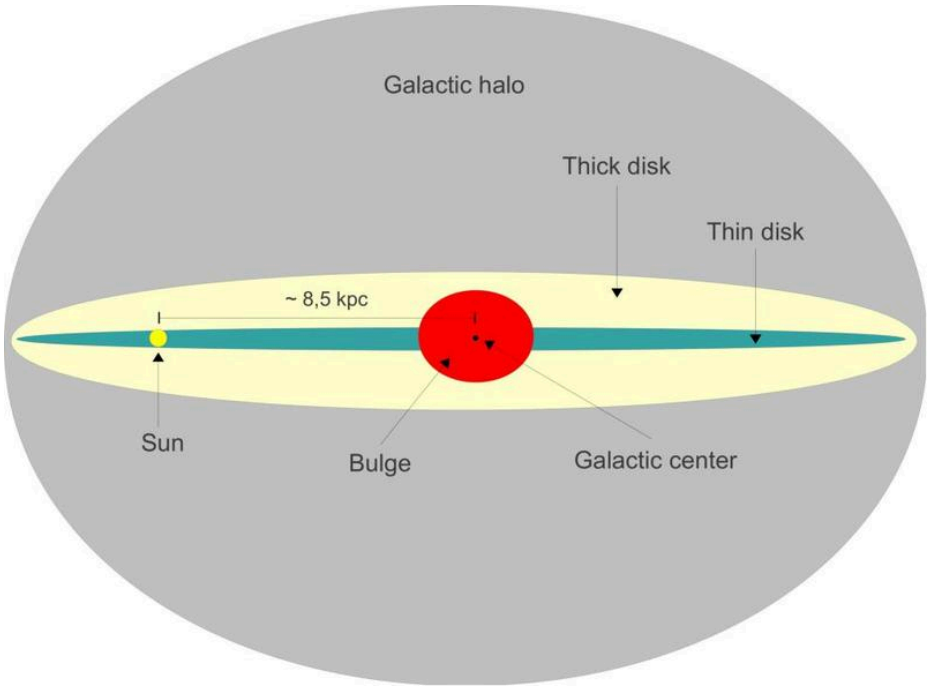

Figure 2.2: Edge-on view of the Milky Way structure (Wikipedia 2017)

The thick disk is a metal-poor region with an unclear origin that is a still a subject of debate. Hosting the oldest stars that were born at an early stage of the formation of the galaxy (7-13 Gyr), the thick disk is the main source of information about the galactic chemical history, through comparative studies with other regions such as the thin disk. The metallicity within the thick disk was found to be quite low i.e $-1 \prec [Fe/H] \prec 0$.
On the other hand, the thin disk is the metal enhanced part of the galaxy ($-0.8 \prec [Fe/H] \prec +0.5$) that hosts the youngest stellar populations.

Galactic disks also differ in the kinematics of the stellar populations that they host. The thick disk stars rotate around the galactic center with $\approx$ 170-180 km/s, slower by 40km/s than the thin disk ones. But, in the vertical direction, with respect to the galactic plane, thick disk stars are found to move faster by 20 km/s. (Bensby 2004).

2.2 Chemical abundances as tracers of galactic evolution

In order to study or model how a given galaxy has formed and evolved over time, it is important to find out how the chemical elements are dispersed in it. The chemical abundance is the measurement of a specific element relative to another one in a particular environment, and in general, relative to solar values. Since the most dominant element in the

Universe is hydrogen, it is often used as the relative element and the chemical abundance could therefore be expressed as the ratio between any element X and e.g Hydrogen such as $[X/H]$. (Matteucci 2012).

In the early stages of the formation of the galaxy, stellar population of high mass stars were the first to explode, emitting many chemical elements (e.g Fe), among them α-elements (e.g O, Mg, Si, Ca, S). In general, α-elements help discriminate between the thin and thick disc and it was found, in many previous studies (e.g Bensby et al. (2004); Ramírez et al. (2013)), that the thick disk has higher [α/Fe] values than the thin disk for given metallicities. The expelled gas from star explosions does not only enrich the interstellar medium but it is also involved in the creation of the next stellar generation. Exploring the trend of alpha elements against the [Fe/H] ratio is a key step in the diagnosis of e.g the the star formation rate (SFR) within a given region of the galaxy. Figure 2.3 below illustrates how alpha elements vary with metallicity as well as different events such as SFR and the initial mass function (IMF), which is a function describing how the mass is distributed within a newly formed stellar population, key parameter in e.g determining the lifetime of a star. When the metallicity is below -0.4, alpha elements show an overabundance, which

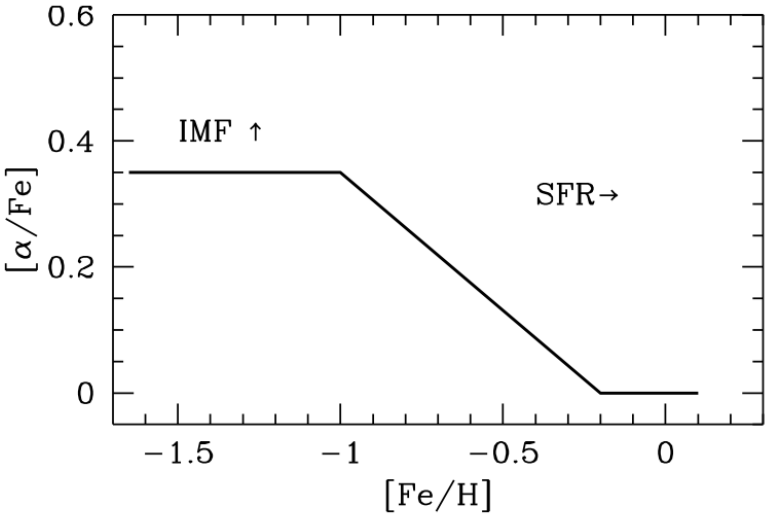

Figure 2.3: Variation of the $[\alpha/Fe]$ ratio with both metallicity and its sensitivity to both IMF and SFR (McWilliam 1997)

means that the region has known events of SN II, hence the positive $[\alpha/Fe]$ values. At this point, the star formation process will continue, thanks to the expelled elements from SN II, until it reaches higher metallicities and as long as SN Ia doesn't take place, otherwise there will be an Fe overabundance, and therefore a drop in α-elements. The down-turn seen on the figure, appears when there is a lack of production of α-elements. Before this happens, the SFR will continue to increase, and the higher the SFR, the more generations

of massive stars will participate in the enrichment with α-elements, making the down-turn further to the right on the plot seen on figure 2.3. (McWilliam 1997)

Concerning the IMF, it is responsible on the position of the constant trend, or the "plateau" at different $[\alpha/Fe]$ values. If the number of high mass stars increases, the interstellar medium will get more chemical enrichment in α-elements from this population since it has a very short life-time. If low mass stars dominate, then the enrichment will be mainly in Fe. The trend in the plateau therefore changes depending on the IMF such that it will be placed at higher levels for dominant populations of high mass stars, and at lower levels if there are more newly born low mass stars. (McWilliam 1997)

Stars that explode as SN II are all massive stars, have shorter life-times than those who explode as SN Ia, and the time delay between SN Ia and SN II is estimated to be 10^8 years (Tinsley 1979), that is why the thick disk for instance is more enhanced in α-elements, which are the main product of SN II, than the thin disk.

Figure 2.4 below (Bensby et al. 2004) represents the resulting $[O/Fe]$ abundances obtained for 72 stars (a combination of solar-type F and G dwarfs in the solar neighborhood) using the 6300Å oxygen line. According to the figure, oxygen is enhanced for thick disk stars and shows lower values for thin disk ones.

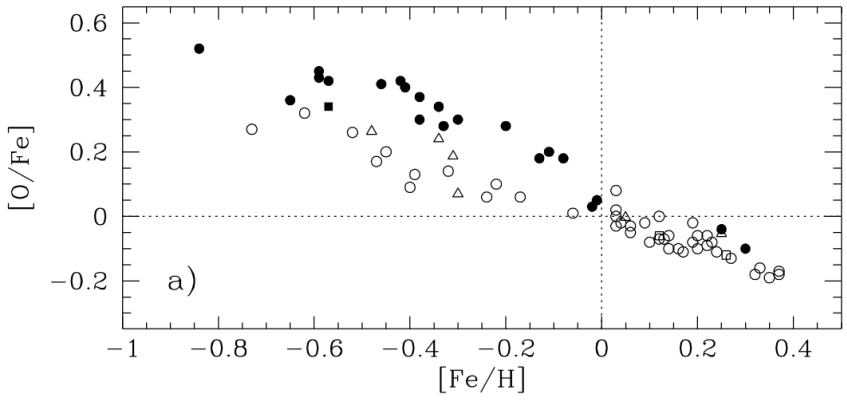

Figure 2.4: Resulting oxygen trend for 72 F and G dwarf stars in the solar neighborhood, using the OI forbidden line marked by circles. Open and filled circles represent thin and thick disk stars respectively. Triangles and squares correspond to results obtained from the triplet lines and the 6363 Å line, respectively.

2.3 The forbidden line

The forbidden oxygen line located at 6300 Å is the most reliable indicator of oxygen abundances (Bensby et al. 2004). Even though this line is weak, blended with a nickel line and suffers from telluric lines due to its location on the spectrum, it represents the huge advantage of being formed under LTE conditions. It is therefore important to correctly take into account all these effects. For instance, observations were conducted using high resolution spectrographs to give spectra as free from noise as possible

In addition, correct atomic data are in this case crucial, especially concerning the nickel blend which must be accounted for, and in particular the oscillator strength $log(gf)$ value, as abundances are particularly sensitive to any errors in this parameter.

Figure 2.5 below (Bensby et al. 2003) shows the forbidden line for three different stars, two of them located in the thick disk (HIP 103458 & HIP 96124) and the other one in the thin disk (HIP 78955), all having different metallicities. The dotted lines represent the nickel blend while the dashed lines are for the oxygen, the solid line is for the combination and finally the circles stand for the observed spectrum. From this fitting it is straightforward to conclude that the spectra concerning stars with lower metallicities, do not suffer from a remarkable nickel blend, and this effect can be neglected. Meanwhile for stars with higher metallicities, the nickel blend gets serious and must be corrected for.

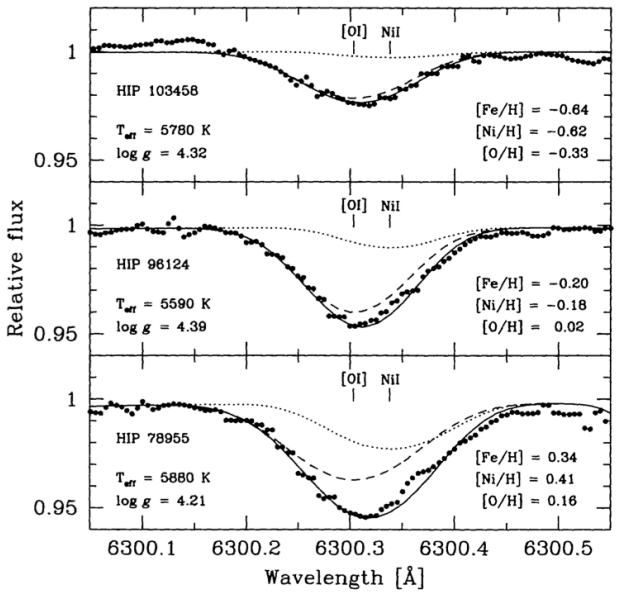

Figure 2.5: The fitting of three synthetic spectra along with an observed spectrum of the oxygen forbidden line at 6300$\mathring{A}$ for three different stars (Bensby et al. 2003)

Moreover, for metallicities $[Fe/H] \geq 0$ the nickel values becomes slightly above solar values (the nickel blend is larger than solar $[Ni/H]$) which could eventually give wrong estimates of the nickel contribution to the $[OI]$6300Å line and therefore a non-reliable estimate of the oxygen abundance. For this reason, nickel abundances were not scaled automatically to solar values. For stars with low metallicity values i.e $[Fe/H] \leq 0$, the nickel contribution to the $[OI]$6300Å line is nearly negligible, so the solar-scaled values for the Ni abundances might be a reasonable approach. This can be further seen from figure 2.6.

Spectral lines get wider as the star rotates faster, and disappear as the rotation reaches extreme velocities; the spectra become too broad to be seen (flat continuum). When light from a rapidly rotating B star passes through Earth's atmosphere, it absorbs whatever elements and molecules it contains. The result will be the flat continuum of the B star along with profiles from Earth's atmosphere, which represent the telluric lines. These lines are also present in any other spectra of stars. In order to get spectral features free from telluric lines, the spectrum of a given star is divided by the spectrum of a rapidly rotating B star. As a result, all the telluric features will cancel out. Since the regarded oxygen line is so weak, this process needs to be done sufficiently carefully to correctly reduce the spectrum. Otherwise, the errors arising from telluric lines have will large effects on the final result coming out from the oxygen line. The radial velocity of the star might change the position of spectral lines but not the telluric ones, which means that the oxygen line in this context might be on the middle or edge of a telluric line, it can even fall under it, or might not be affected at all.

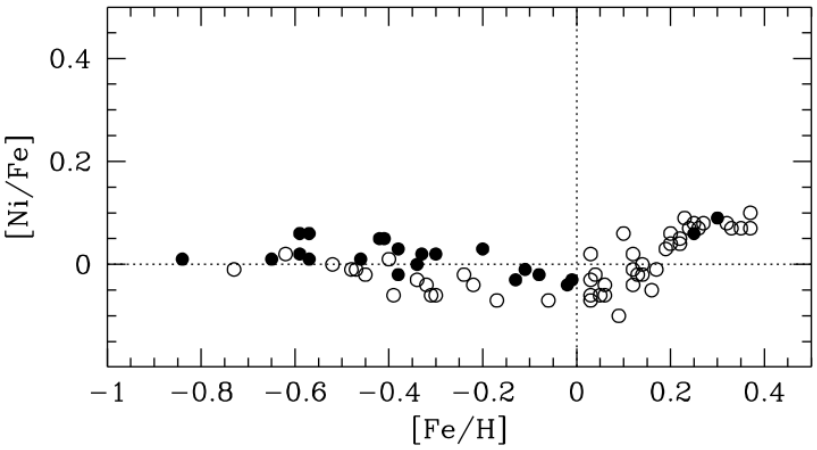

Figure 2.6: Observed nickel trend for a sample of 72 F and G dwarf stars in the solar neighborhood. Open and filled circles correspond to respectively thin and thick disk stars. (Bensby et al. 2004)

2.4 The triplet lines

Other methods for determining Oxygen abundances include the equivalent width measurements of the oxygen infrared triplet lines located at 7770Å-7775Å present in figure 2.7 (Sneden et al. 1979) for two different stars, they are strong and non-blended but suffer from Non-LTE conditions.

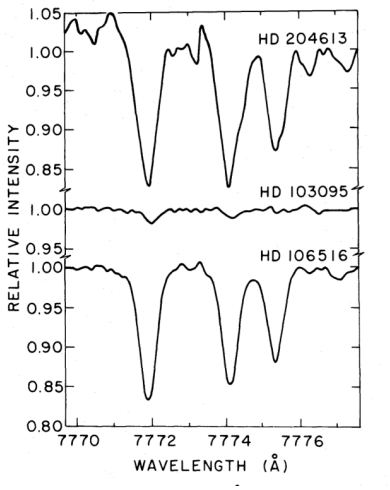

Figure 2.7: Examples of spectra of the oxygen triplet lines with different strengths (Sneden et al. 1979)

Local thermodynamic equilibrium:

Radiative transfer describes the energy transfer as an electromagnetic radiation. This phenomenon can be affected by several processes such as; emission, absorption and scattering of particles within a medium. Solutions for this problem are somehow complicated. Nevertheless, an assumption of Local Thermodynamic Equilibrium condition (LTE) is very helpful. In this situation, the particles that make up the gas of the medium are only characterized by a local temperature. The flow of these particles into any energy level is compensated by the inverse flow in the same level, e.g any absorption is balanced by an emission.

Departures from LTE conditions produce many complexities on stellar spectra. This case occurs when assumptions of LTE cannot be valid. However, empirical corrections to LTE conditions are fortunately possible, and can be derived if both forbidden and triplet lines are analyzed in the same stars. These corrections rely on the comparison of oxygen abundances from the triplet lines to those derived from the forbidden line. (Bensby et al. 2004). When these corrections are applied, the analysis based on the triplet lines can therefore become reliable. Further proper and full NLTE treatments are possible but more complicated and time-consuming, the oxygen abundance calculations from the triplet lines

are required to be done across a 3 dimensional hydrodynamic stellar model atmospheres e.g the STAGGER grid, which represents a more realistic model (Amarsi et al. 2016).

Chapter 3

Method

Oxygen abundances were obtained from the synthetic spectral fitting of the oxygen forbidden line at 6300Å. The analysis was based on a high resolution spectra for a subset of the 714 stars in the Solar neighbourhood presented by Bensby et al. (2014).

3.1 Stellar sample

The data used during the analysis consists of 714 F and G type dwarf stars taken from (Bensby et al. 2014), which were mainly selected for the purpose of studying the abundance structure of the thin and thick stellar disks of the Milky way. These stars are similar to the Sun (in temperature and surface gravity) and so they are easier to analyze than e.g giant stars. They are main-sequence, turn-off and subgiant stars, therefore estimates of their ages can be estimated from isochrone fittings, varying between ≈ 2 billion years to as old as the oldest stars (≈ 13 billion years). They stay on the main-sequence approximately 10 Gyr, during this time their atmospheres remain intact. This means that they hold information about the history of stellar populations. This can be revealed through finding out the mix of chemical elements that the gas cloud contained, which formed the stars billions of years ago.

High resolution spectra with high signal to noise ratio (S/N) were obtained from the ESO 6.5-m Magellan telescopes in Las Campanas and the ESO 8.2-m Very Large Telescope (VLT) in Paranal, which represent the world's largest telescopes, all located in Chile.

Out of the 714 stars, only 485 were suitable for the analysis at 6300$\mathring{A}$, which were observed with the MIKE spectrograph. These spectra have signal to noise (S/N) ≈ 200 (Bensby et al. 2014) and the highest resolution that ranges between 40000 and 65000, suitable for the weak oxygen line. In addition, all these spectra were divided by a rapidly rotating B star to exclude telluric lines.

3.2 Line synthesis

Since the forbidden line is very weak and blended by a Ni line, the method of equivalent-width measurement is not suitable to carry out the abundance study. Instead, line synthesis is more appropriate, since it takes into account the weakness and blends of the line. The resulting spectra were then compared to the observed spectrum to find the best fit. The synthetic spectra were calculated using the SME package.

SME (Valenti & Piskunov 1996), is a software package that represents a powerful tool that helps fitting observations with synthetic spectra for a given set of input parameters and abundance interval with a step size. During the analysis, SME used the MARCS model atmospheres (Model Atmospheres in Radiative and Convective Scheme created by Gustafsson et al. (2008)).

Before this can be done, SME needs a number of input data such as the atomic line data, which include for each element; the wavelength, excitation energy, oscillator strength, radiation, Stark as well as Van Der Waals damping constants, and finally the Lande factor, which is a dimensionless physical quantity that relates the magnetic moment to the angular momentum of a quantum state. This data was queried by the VALD database for the relevant wavelength range, in which the OI line was created manually. SME also needs the stellar parameters, which were obtained from Bensby et al. (2014), and include; Effective temperature, surface gravity, solar abundances (of any other element relevant to the targeted study i.e Fe, Ni, Si, etc), the final rotation and the micro-turbulence, which is a form of turbulence that varies over very small distances, comparable to the mean free path of a photon.

3.3 Procedure

In order to calculate the O abundances from the forbidden line, a software was used to carry on the spectral fitting of the observed and synthetic spectra, in which all the needed input data was defined, including a section in which it relies on the SME package to receive the synthetic spectra. Figure 3.1 below is a flowchart that briefly describes the major steps that the script from ESO-MIDAS (European Southern Observatory-Munich Image Data Analysis System) adopts to proceed the analysis. The major steps numerated from 1 to 11 are described below.

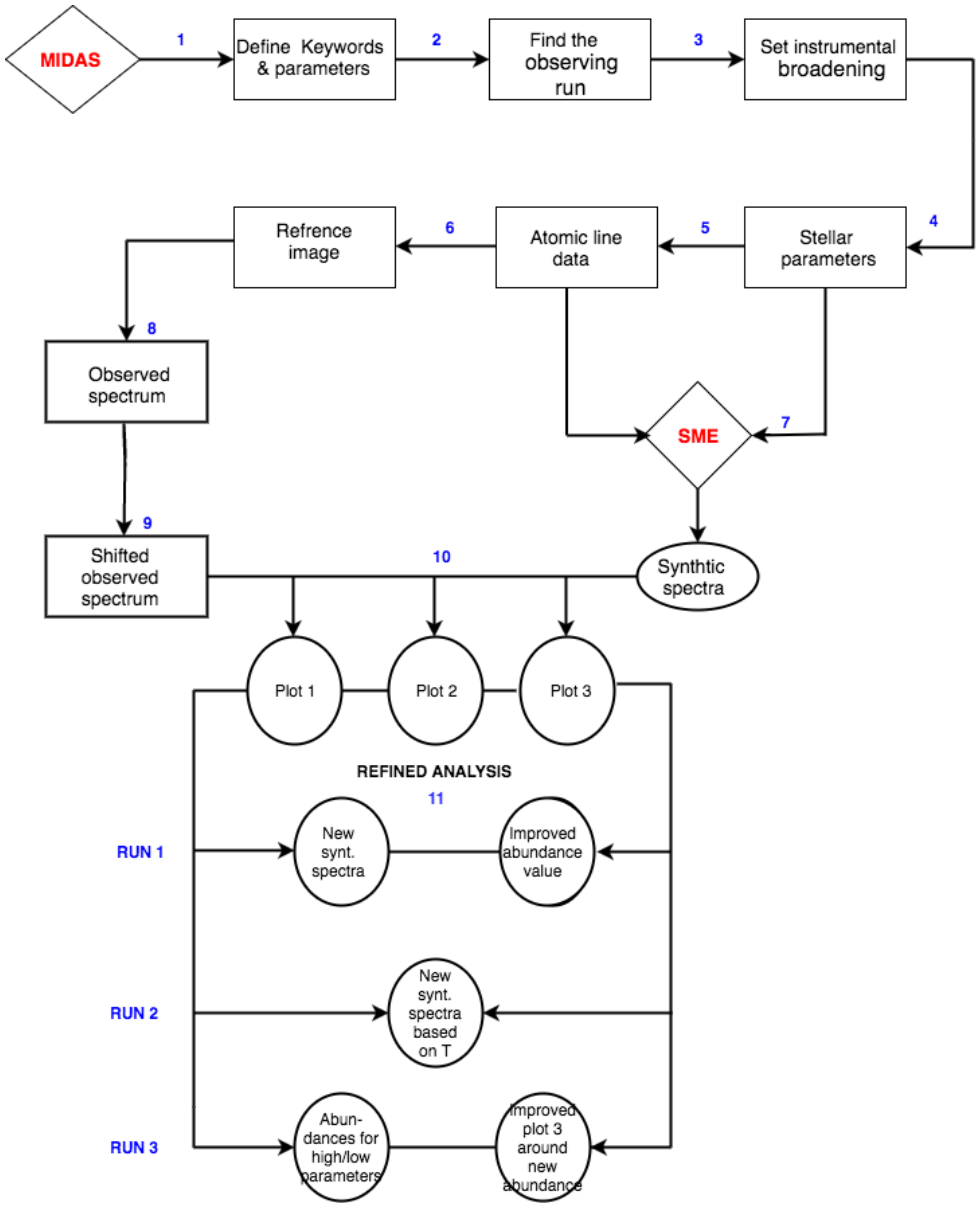

Figure 3.1: MIDAS script flowchart

1. The script starts by defining all the parameters and keywords used in the script.
2. Find the observing run from the Hipparcos ID of the star, if the ID number (e.g star number 80) was not given or was not valid, the analysis jumps to the end of the script directly and ask for a new HIP ID.

3. Set the instrumental broadening: Define which type of instrument was used during the observation depending on the resolution of the observed spectrum.

4. Find the following stellar parameters: The effective temperature T_{eff}, surface gravity $log\ gf$, micro-turbulence, metallicity, $[Ni/H]$. For each the errors were also defined. Also, the velocity shift of the spectra and final rotation for each star were defined.

5. The VALD database was used to get the atomic line data. The requested line list was in the interval [6290Å,6325Å]. A set of about 50 lines from many elements was obtained along with their output parameters that include; the oscillator strength $log(gf)$, wavelength, excitation energy, etc.
Wavelength intervals were defined as [6290.3Å, 6320.3Å], for starting and ending wavelengths, and [6296.3Å, 6304.3Å] for the maximum and minimum values, central $\lambda = 6300.3$Å as well as the continuum levels on both left and right parts of the synthetic spectrum.

6. The wavelength intervals defined previously were used during this step to create a reference image. It will be needed for the script to correctly project the output image on a spectrum, so that both the observed spectrum and synthetic spectra have the same scale.

7. SME takes the stellar parameters and atomic line data, a wavelength interval [6296.3Å, 6304.3Å] and resolutions of the spectra. Based on this information, and a grid of model atmospheres (MARCS from Gustafsson et al. (2008)), SME calculates the synthetic spectra.

8. Make sure that both spectra have the same binning and step sizes for the data points, so that it can calculate the differences between the observed spectrum and each of the ten synthetic spectra.

9. A wavelength shift was applied to the observed spectrum so that it is horizontal and lies on the same level as the synthetic one. It will be rectified in case it has a slope by doing a linear regression.

10. In this step, the program makes three graphs as shown below in figure 3.2; a plot of both the observed and synthetic spectra (plot 1), a plot of their differences (plot 2) and plot of $sum(\chi^2)$ values against $log(\epsilon\ O)$ (plot 3). $sum(\chi^2)$ represents the squared difference between each synthetic and observed spectrum. The program defines a tables with two columns, one containing values of $sum(\chi^2)$ and the other containing the ten defines abundances. It finds the best oxygen abundance value by matching it to the minimum value of $sum(\chi^2)$.

11. Start of the **refined analysis** This step was done following four different runs such that:

Run 1: The script takes the first best abundance, and does a refined analysis around this value while taking into account the low and high errors in temperature $T_{eff-low}$ and $T_{eff-high}$, which gave an output of two more new best abundance values; for both a low and high errors in temperature.

Run 2: The effective temperature was set back to its normal value T_{eff} and the errors in $log(g)$ were considered, i.e $log(g)_{low}$ and $log(g)_{high}$. The refined analysis gave two new best abundance values relative to errors in the surface gravity; one for $log(g)_{high}$ and the other for $log(g)_{low}$.

Run 3,4 & 5: The same scenario was repeated in the exact same fashion, taking in consideration the low and high errors in $[Fe/H]$, $[Ni/H]$ and the micro-turbulence, respectively. Therefore, six more abundance values were obtained.

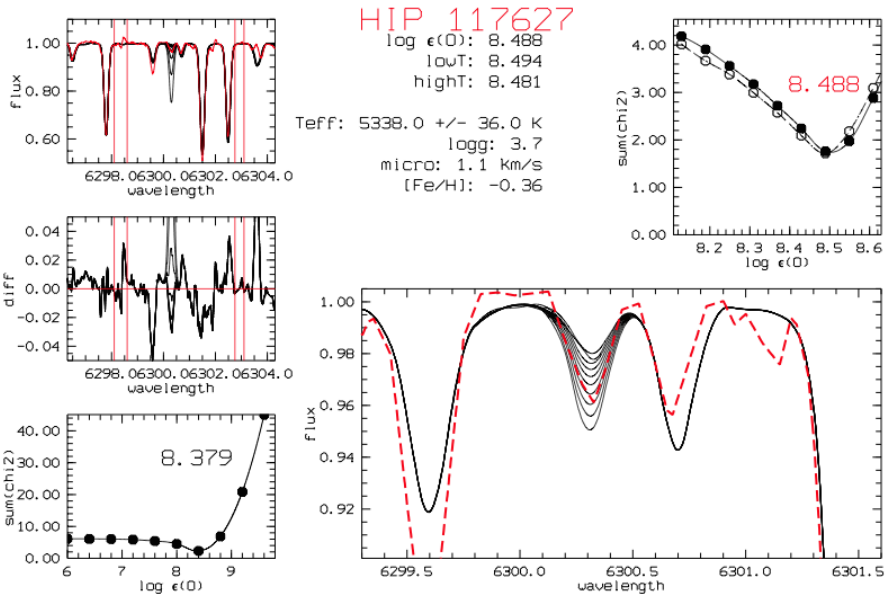

Figure 3.2: MIDAS output graphical window. This was obtained from the analysis of the star with Hipparcos ID 117627. The window shows three different plots on its left side, these were obtained from step 10 in the flowchart and they represent the preliminary resulting oxygen abundances before the start of the refined analysis, which aims at improving the abundance values by taking into account the uncertainties, and therefore obtaining a better abundance plot and spectral fitting. The window is also labeled with the effective temperature and its error $T_{eff} = 5338.0 \pm 36.0K$. The new best abundance variation with respect to both $5856.0K + 47.0K$ and $5856.0K - 47.0K$ (lowT and highT), as well as the value of the star's surface gravity $log\ (g) = 3.7$, the micro turbulence $1.12km/s$ and finally the star's metallicity $[Fe/H] = -0.36$.

3.4 Solar abundances

The results obtained from the calculations carried by the routines described in the previous section, are absolute abundance values, expressed in dex, and defined as the following:

$$\epsilon(X) = log(N_X) - log(N_H) \tag{3.1}$$

Where N_X is the number density of atoms for a given element, and N_H is the number density of atoms for hydrogen.

It is more useful to use use solar normalized values, meaning abundances relative to the Sun. That is since the Sun's chemical composition is known. These values were obtained by applying the following expression:

$$[O/H] = \epsilon(O)_{star} - \epsilon(O)_{\odot} \tag{3.2}$$

Where $\epsilon(O)_{star}$ is the absolute abundance of oxygen in a given star and $\epsilon(O)_{\odot}$ is the absolute oxygen abundance in the Sun derived from the $[OI]6300$Å line, which was determined during this study via five spectra, from both Ganymede (Jupiter's largest moon) and Ceres, largest planet found within the asteroid belt. The reason for this was to decrease the uncertainty of the final result, other results from previous studies might come from different models that do not match the method adapted here (e.g using a different spectral line). However, the absolute O abundance value derived for the Sun, $\epsilon(O) = 8.63$, matches pretty well the value derived by Allende Prieto et al. (2001), which is $8,69 \pm 0.05$.

3.5 Uncertainties

The oxygen uncertainty calculations were done in the script, by varying the stellar parameter with their errors, and the oxygen abundances were calculated relative to each one of them, for both the low and high values (i.e plus and minus the error values). The stellar parameters that were considered to include; effective temperature, surface gravity, nickel and iron abundances as well as the micro-turbulence. Values for these errors were taken from (Bensby et al. 2014). The total uncertainty in the derived oxygen abundance, which assumes that the errors are uncorrelated, is expressed as:

$$\Delta(O) = \sqrt{\Delta^2_{T_{eff}} + \Delta^2_{log((g)} + \Delta^2_{[Fe/H]} + \Delta^2_{[Ni/H]} + \Delta^2_{micro}} \tag{3.3}$$

But this is only the random error in stellar parameter. Inaccuracy in the final result might also arise from the spectral fitting procedure, the observed spectrum and synthetic spectra must fit well for a reliable calculation. In case the spectra don't fit the star will not be used for the analysis. The continuum level has to be carefully placed, from well-defined regions on the spectrum that contain no lines at all.

Telluric lines, which arise as a result of the spectral lines entering Earth's atmosphere, cause large uncertainties when not correctly taken into account.

Chapter 4

Results

4.1 Oxygen abundances

In table 4.1 below we represent a sample of the results acquired from the calculations done using the ESO-MIDAS software, for only ten stars out of 485 that were analyzed. These include the value of the absolute oxygen abundance after the refined analysis for each star. As well as the abundances with respect to plus and minus the errors in each stellar parameter individually, e.g highT stands for the absolute oxygen abundance when the plus error in the effective temperature is taken into account, lowT for minus the error. Also, G, F, N and M respectively stand for the abundances when accounting for the uncertainties in the, surface gravity log g, $[Fe/H]$, $[Ni/H]$ and the micro-turbulence.

Figure 4.1 below is a representation of how the iron abundance varies depending on the oxygen abundance. According to this result, the O production increases with increasing Fe production.

Table 4.1: Calculated results for absolute oxygen abundances before and after the refined analysis and for uncertainties in different stellar parameters for 10 out of 485 stars

HIP ID	log ϵ (O)	highT	lowT	highG	lowG	highF	lowF	highN	lowN	highM	lowM
80	8.60	8.63	8.64	8.65	8.63	8.63	8.62	8.63	8.62	8.63	8.65
305	8.95	8.97	8.96	8.96	8.96	9.06	9.00	8.88	8.96	8.96	8.90
407	8.85	8.86	8.85	8.85	8.85	8.85	8.91	8.78	8.85	8.85	8.76
1349	7.97	7.97	8.22	8.22	8.22	8.22	8.12	7.97	8.22	8.22	8.22
1746	8.77	8.80	8.87	8.78	8.78	8.78	8.8	8.76	8.78	8.78	8.76
1877	8.49	8.50	8.4	8.4	8.4	8.4	8.84	8.77	8.81	8.12	8.74
1931	8.87	8.90	8.89	8.89	8.89	8.89	8.97	8.81	8.9	8.89	8.76
1955	8.77	8.81	8.81	8.81	8.81	8.81	8.84	8.77	8.81	8.81	8.74
1976	9.02	9.05	9.03	9.03	9.03	9.03	9.07	9	9.03	9.03	9.08
2057	8.52	8.53	8.53	8.53	8.53	8.53	8.55	8.494	8.53	8.53	8.43

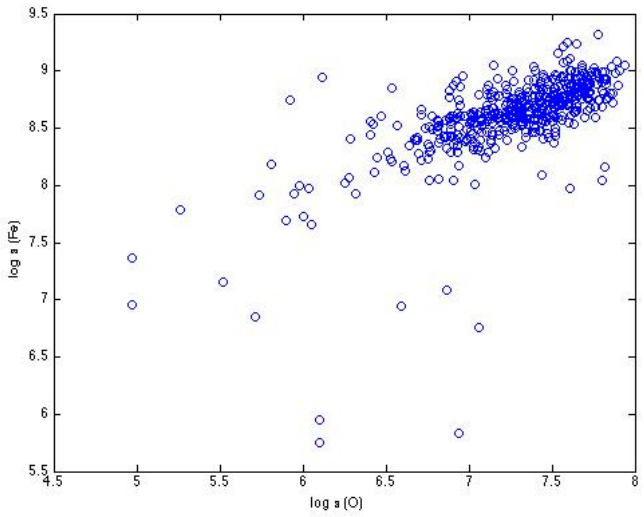

Figure 4.1: Variation of the absolute oxygen abundance with respect to the absolute iron abundance

The analysis of five spectra, two from Ganymede and three from Ceres, gave an average absolute oxygen abundance in the Sun of about $log\epsilon(O)_{\odot} = 8.63$. The individual values for each body are found in the table 4.2 below, along with the variation with each stellar parameter.

Table 4.2: Calculated results for absolute oxygen abundances for the Sun, after the refined analysis and for uncertainties in different stellar parameters

	log ϵ (O)	highT	lowT	highG	lowG	highF	lowF	highN	lowN	highM	lowM
Ganymede 1	8.61	8.60	8.66	8.60	8.64	8.64	8.64	8.64	8.61	8.67	8.64
Ganymede 2	8.75	8.72	8.76	8.72	8.75	8.75	8.75	8.75	8.75	8.79	8.75
Ceres 1	8.66	8.86	8.85	8.85	8.85	8.85	8.91	8.78	8.85	8.85	8.76
Ceres 2	8.66	8.49	8.56	8.49	8.85	8.85	8.50	8.50	8.48	8.57	8.50
Ceres 3	8.61	8.59	8.62	8.59	8.61	8.61	8.61	8.61	8.58	8.62	8.61

4.2 Oxygen abundance trends

The results derived using the oxygen forbidden line were compared to results obtained using the triplet lines from a previous analysis in Bensby et al. (2014), for stars found within the same sample. The sample was divided into two sub-samples in order to discriminate for the thin and thick disks, based on stellar ages on one hand, and kinematics on the other hand. Stellar ages and kinematics were obtained from Bensby et al. (2014).

The kinematical selection was based on the probability TD/D, thick disk to disk ratio. Using known space velocities for each star, the probability for belonging to either the thin or thick disks can be calculated, based on the kinematical proprieties of the disks. If $TD/D > 2$, then the star most likely belongs to the thick disk. Automatically, thin disk stars have lower values of about $TD/D < 0.5$. The age criterion was set for stars older than 8 Gyr and younger than 7 Gyr, for respectively thick and thin disk populations. In all resulting figures below, red circles and blue stars represent the thin and thick disk stars, respectively.

The results in both figure 4.2 and 4.3 rely on age criteria to divide the sample. In figure 4.2, there is an obvious overlap in abundance space. While in figure 4.3, the stellar populations are more distinguished. There is an obvious trend of metal-rich and less oxygen enhanced population, which correspond to the thin disk, as well as a metal-poor and oxygen rich population, namely the thick disk.

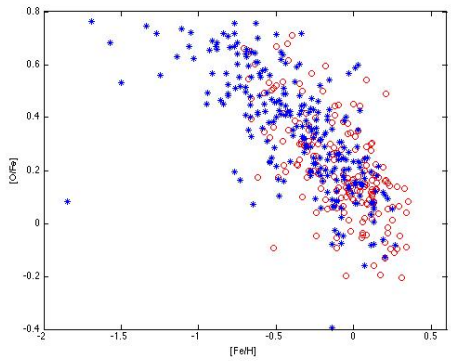

Figure 4.2: Obtained [O/Fe] trend with respect to [Fe/H] from the oxygen forbidden line, based on the age criteria. Blue stars and red circles correspond to respectively the thick and thin disks.

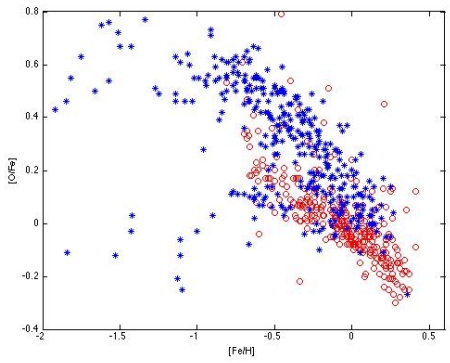

Figure 4.3: Obtained [O/Fe] trend with respect to [Fe/H] from the oxygen triplet lines, based on the age criteria. Blue stars and red circles correspond to respectively the thick and thin disks.

For the kinematical selection, stars that are twice more likely to be thick disk stars (blue) than thin disk stars (red) are supposed to be more oxygen enhanced. For both results obtained from the forbidden and triplet lines, there are few thick disk stars that fall below the zero $[O/Fe]$ level, while there are many thin disk stars that show thick disk kinematics. The overlap in both figures results from the fact that the sample contains

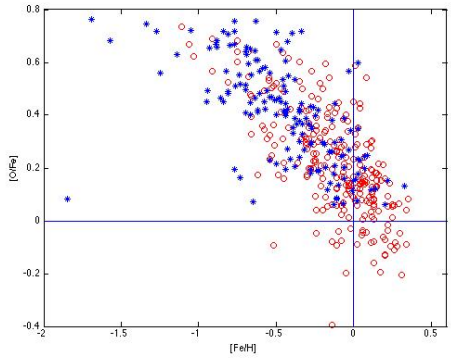

Figure 4.4: Abundance trends for the oxygen forbidden line using kinematical criteria. Blue stars and red circles correspond to respectively the thick and thin disks.

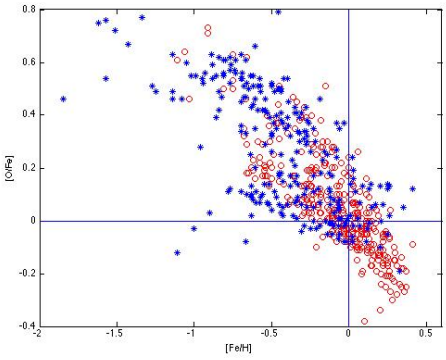

Figure 4.5: Abundance trends for the oxygen triplet lines using kinematical criteria. Blue stars and red circles correspond to respectively the thick and thin disks.

many stars with thick disk kinematics at high metallicities, as well as stars with thin disk kinematics at low metallicities.

After testing both selection criteria based on the 6300Å and triplet lines, it is notable that the forbidden line is not at all able to chemically separate the thin and thick disks. In fact, the triplet lines have shown better results in discriminating between thin and thick disk stellar populations, as the chemical trend present for the triplet lines in figure 4.3 is much cleaner. This was an unexpected result, and the reasons that led to this case need to be further investigated.

4.3 Oxygen as a proxy for age

Many previous studies (e.g Bensby et al. (2014); Haywood (2012)), have found that α-elements can be used as a proxy for stellar ages, since the structure of their distribution among the Milky Way disk is quite well-known. This section is a check if the same assumption is valid for oxygen. Abundances were used from both the forbidden and triplet lines. As seen from figure 4.6, this is only valid for stars with ages older than 8-9 billion years. There is no trend for young stellar populations. So oxygen can only indicate ages when the stellar populations belonging to the thick disk are concerned. This is due to the fact that O is only enhanced for stars that are are older, and has low abundances for thin disk stars. On the other hand, the forbidden line as previously shows no accurate results in figure 4.7.

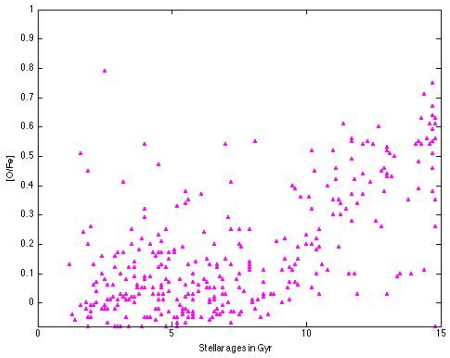

Figure 4.6: [O/Fe] versus stellar ages, expressed in billion years, only for stars with low uncertainties, less that 4 billion years, case of the triplet oxygen lines.

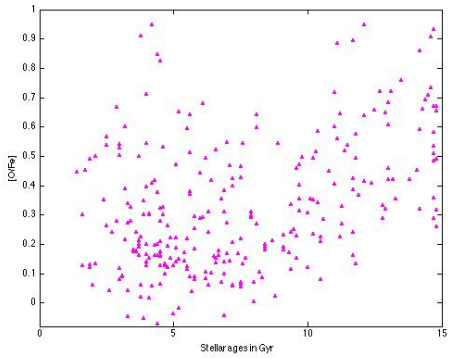

Figure 4.7: [O/Fe] versus stellar ages, expressed in billion years, only for stars with low uncertainties, less that 4 billion years, case of the forbidden oxygen line.

4.4 Errors in resulting abundances

The deviation between the results obtained from the forbidden line and the triplets is shown in the figure 4.8 below. The standard deviation between the results obtained from both methods was calculated to be $< [O6300\text{Å}/O7774\text{Å}] >= 0.3 \pm 0.1 dex$.

Furthermore, a specific deviation was plotted in figure 4.9 between the results from the two methods, for three different stellar parameters; effective temperature, metallicity and surface gravity. In this case too, no trend seems to explain the difference as the two methods seem to give nearly similar results with respect to the three different parameters.

The uncertainty in the derived O abundances, with respect to each stellar parameter is shown below in figure 4.10. The error in this case, was investigated by varying the parameter in question, and as we can see from the figure, the oxygen abundance is affected differently depending on the varying parameter. Here, $\Delta(O)$ is defined as half the difference between the values of the derived oxygen abundances relative to high and low errors, of one of the given parameters. For instance, variations were seen for errors arising from the micro-turbulence, and the standard deviation of the result in this case was estimated to 0.06 ± 0.03dex. The scatter of the abundances due to errors in the metallicity and effective temperature are quite similar, the standard deviation is respectively 0.05 ± 0.03dex and 0.05 ± 0.02dex. There was no error due to surface gravity at all, and the offset of the oxygen abundance due to uncertainty in the nickel abundance was estimated to 0.08 ± 0.05dex.

Another suggestion to reveal the reason behind the faulty distinction between the disks when relying on the forbidden line, is to look back at the data reduction for telluric lines. Figure 4.11 shows how the telluric lines are placed on the spectrum of an example star (black lines), and figure 4.12 is the spectrum free of telluric lines after the division. This example concerns the observed spectrum for only one star. In case this procedure was not

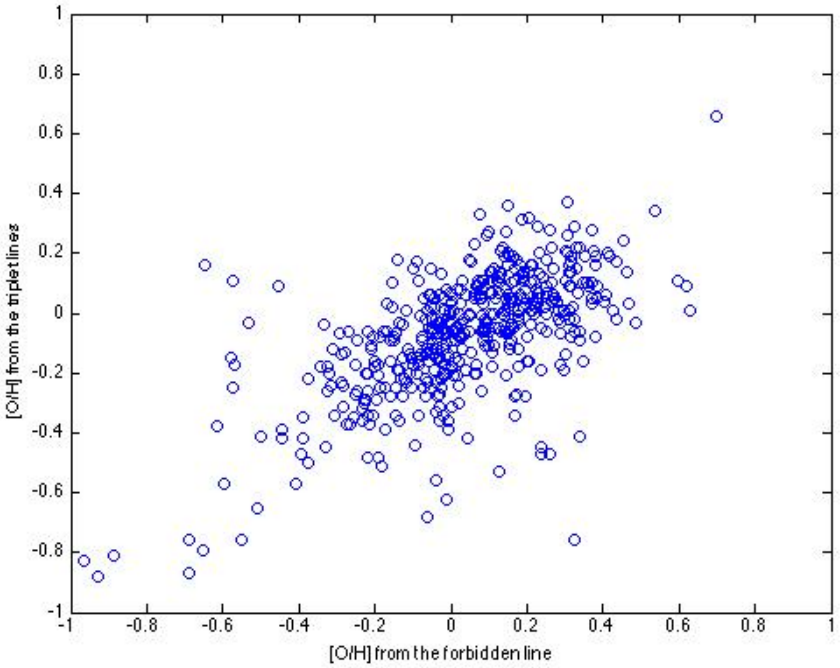

Figure 4.8: Results obtained using the forbidden line with respect to results from the triplet lines

precisely done for the entire sample, the oxygen line would have been smeared out by a telluric line, and hence the faulty derived abundances.

In addition, the spectral fitting was not exactly perfect for a large number of stars, and some spectra suffered from a lower (S/N) relative to others. This can be seen from figure 3.2 above, where the MIDAS output graph is displayed. The observed spectrum (red), does not exactly fit to the synthetic spectrum, especially when approaching the $6299.7-6300.5$Å wavelength region. The noise rather appears around 6300.9Å.

Finally, the error due to the atomic data in general, and due to the oscillator strength ($log(gf)$-values) in particular, are the most important. Any deviation from the correct value, in this case, will not completely take into account the nickel blend, and one ends up with a spectrum that still suffers from the presence of another element in its oxygen line, which of course will result in wrong abundances that do not represent the oxygen alone.

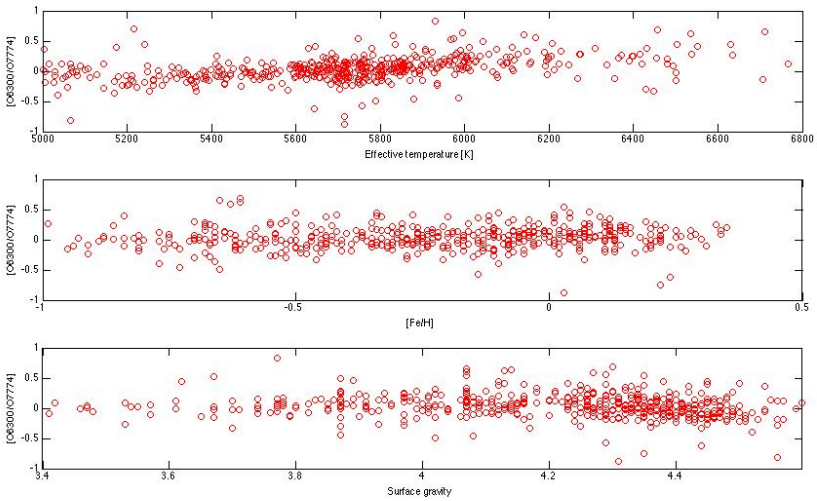

Figure 4.9: Results obtained using the forbidden line with respect to results from the triplet lines, with respect to effective temperature, metallicity and surface gravity

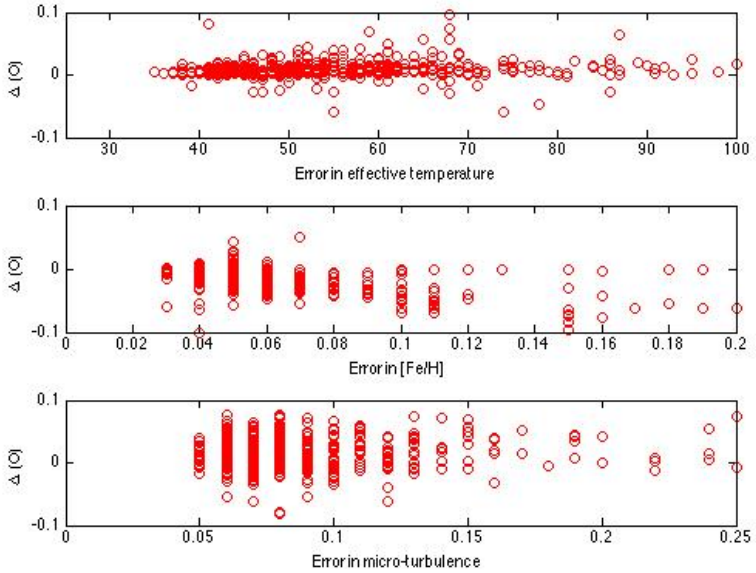

Figure 4.10: Variation of the oxygen abundance depending on the error in each stellar parameter; the effective temperature, surface gravity, metallicity and micro-turbulence

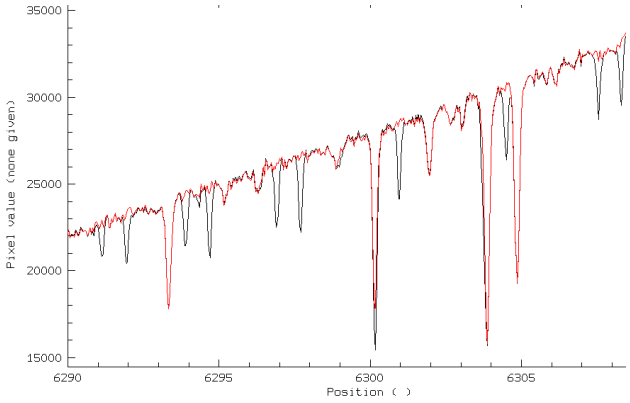

Figure 4.11: Position of the telluric lines (black) on the observed spectrum (red) before data reduction

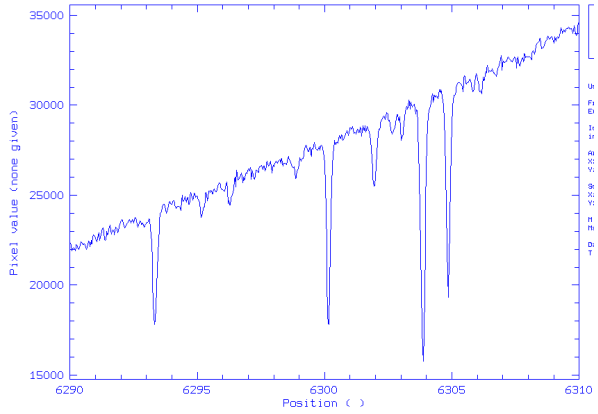

Figure 4.12: Observed spectrum after reduction from telluric lines

4.5 Discussion

Oxygen abundances obtained in this study from the forbidden line at 6300 Å for the sample of 714 F and G dwarf stars in the solar neighborhood shows difficulty in tracing thin and thick disk stellar populations, both when using the age and kinematical criteria. The triplet lines located at 7774 Å, in contrast, are able to do so. It is currently unclear why this is the case, but there might be several different reasons.

Sources of errors such as the stellar parameters cannot be a possible cause for such a huge deviation. As a matter of fact, the same stellar parameters were used for the analysis from the triplet lines and the resulting O abundances obtained previously in Bensby et al. (2014) have been successful for tracing the thin and thick disk stellar populations, as shown in figure 4.3 and 4.5 above. Also, the total random uncertainty in O abundances from the

6300Å line arising from stellar parameters was estimated to approximately 0.05 dex, which is not enough to wash out the signatures of the Galactic disks. The same applies to the spectral fitting, which was done in a fairly precise way in which spectra were verified one by one throughout the analysis to make sure that the fitting procedure was done correctly. The noise that originates from the observed spectrum, cannot cause too much error neither.

This could also be partially due to the continuum placement which was done during the analysis. Small shifts in the continuum levels give a huge impact on the O abundances because the 6300Å line is too weak.

Another possibility concerns the spectral quality, which might not be sufficient enough. The OI line at 6300Å is too weak, and therefore higher resolutions and signal-to-noise ratios are crucial in order to obtain accurate results. In addition, the blend of this line must be taken into account by feeding the atomic line data with the right nickel oscillator strength, which must be as accurate as possible.

The forbidden line has shown the same difficulty in chemically separating the disk in a previous study by Bertran de Lis et al. (2015). Figure 4.13 below shows too much overlap, due to the difficulty of this line to achieve a correct separation.

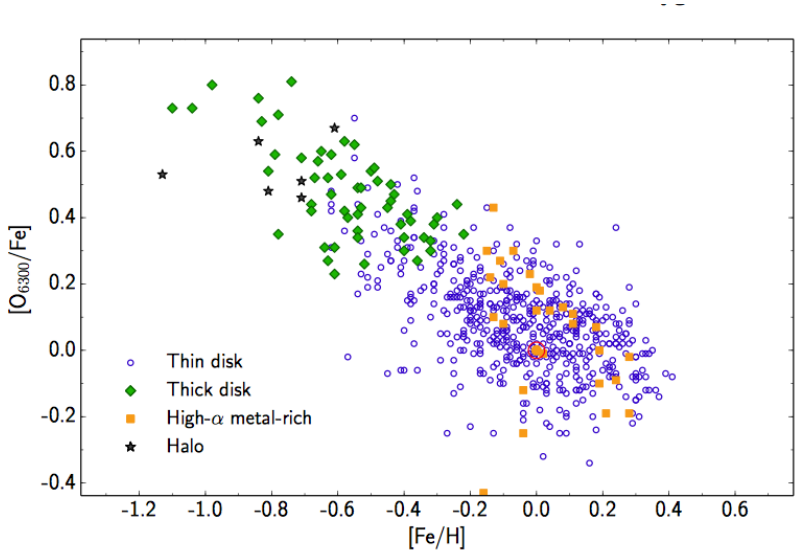

Figure 4.13: The [O/Fe] versus [Fe/H] trend obtained from the analysis of the oxygen forbidden line for a sample of 610 solar-type dwarfs and sub-giants (Bertran de Lis et al. 2015)

Chapter 5

Summary and conclusions

oxygen, with atomic number 8, is mainly produced inside massive stars through processes of stellar nucleo-synthesis, and expelled into the interstellar medium via star explosions, more particularly supernovae type II, which involves the collapse of a massive star. This element can trace stellar populations belonging to thin and thick disk regions of the Galaxy. Through comparative studies with mainly iron, O can reveal help with e.g revealing the formation timescale for both disks as well as serve as a proxy for stellar ages. Galactic formation, history and evolution, is a vast branch of Astrophysics that has for long been a subject of research and debate, and which will continue for many years into the future. To answer the mystery of how our Galaxy has formed, spectroscopic studies of stellar populations in the Milky way have been conducted to reveal the chemical mix out of which these stars are made of, as the chemical abundance is a tracer of chemical evolution. This project is particularly targeted to study how oxygen varies within stellar populations in the solar neighborhood.

To make this study possible, 714 F and G type dwarf stars in the solar neighborhood have been observed from one of the World's largest telescopes in order to collect high resolution spectra. On these spectra, oxygen lines appear at different wavelengths, namely 6300Å, $7771 - 7774$Å and 6363Å, out of which the 6300Å has so far shown more or less reliable results, and which was used to determine the O abundances during this project, that aims at testing the reliability of this line for the sample in question, by comparing the final result to the results previously obtained from the triplet lines. The forbidden oxygen line is very weak and blended with a nickel line, but unlike the triplet lines located at $7771 - 7774$Å, it is not sensitive to NLTE conditions, which presents an benefit quality. The calculations were then carried by the spectral fitting of the observed and synthetic spectra of each star.

Stellar parameters have been already determined as precisely as possible, in Bensby et al. (2014), in which the stellar sample, containing both oxygen indicators, was subject to a data reduction. The atomic line data for the sample were directly obtained from an online database named VALD.

The analysis was done only on spectra obtained with the Mike spectrographs, which was a total of 485 stars in the sample. This instrument has a high resolution, up to 65000,

and therefore suitable for the forbidden line which is severely weak. The results from the adapted routine included absolute oxygen abundances, as well as these values relative to plus and minus the errors in each stellar parameter.

The abundances obtained for the 485 stars had to be normalized to oxygen solar values. As a consequence, a solar analysis was performed on five spectra from observations done on both Ganymede and Ceres following the same routine as for the 485 stars. Previously calculated oxygen solar values could have been used, but this option was avoided to minimize the final uncertainties, which can arise from using other results obtained from different methods.

After performing an analysis on these results obtained via the forbidden line, it turned out that this indicator fails at chemically tracing the thin and thick disk stellar populations, for the sample in use. The distinction between the two populations could be based on either the age or kinematical criteria, since these proprieties differ totally for both populations. Graphs that aimed at viewing this separation showed too much overlap and there is almost no distinction at all between the disks. However, the exact same procedure was also performed using the triplet lines, and the results were rather reliable.

Calculated uncertainties due to the stellar parameters and atomic line data were not large enough to wash out the trend. For instance, there is almost no dispersion at all due to surface gravity, and errors in e.g metallicity and effective temperature were quite small. This shows that the problem goes back to either the sample or the analysis routine. The sample was probably not of sufficient quality to obtain reasonable results from the very weak line at 6300Å. Moreover, if the continuum level was not correctly placed on the spectra then it definitely is the cause of this uncertainty.

Studies of how the oxygen abundance trend varies within the Galactic thin and thick disks indicate that these two regions have had different histories and chemical evolution processes that lead to their present distinct proprieties. These include the ages of the stellar populations that they host, such that the thick disk contains stars with ages varying from nearly 8 billion years to the oldest stars, while the thin disk is home for relatively younger populations. Furthermore, the oxygen underabundance in the thick disk is a proof that this region has acquired its chemical enrichment more from supernovae type Ia than supernovae type II, and vice versa for the thin disk, which is more oxygen enhanced.

Appendix

The atomic line data obtained via VALD is the following:

```
    6290.00000, 6310.00000, 49, 1841, 1.0, Wavelength region, lines selected, lines processed,
                  Vmicro
                                                    Damping parameters  Lande  Central
Spec Ion      WL_air(A) Excit(eV) Vmic log gf*  Rad.  Stark  Waals factor  depth  Reference
'Fe 1',      6290.5427,  2.5881, 1.0, -4.330, 8.250,-6.060,-7.570, 1.370, 0.048, '  1 K14
'Si 1',      6290.7426,  6.0827, 1.0, -2.017, 9.160,-3.150,-7.250, 1.530, 0.033, '  4 K07
'Si 1',      6290.7913,  6.0787, 1.0, -1.074, 9.040,-2.710,-6.990, 0.530, 0.189, '  4 K07
'Fe 1',      6290.9647,  4.7331, 1.0, -0.771, 8.400,-4.660,-7.510, 1.640, 0.399, '  1 K14
'Nd 2',      6292.8160,  0.1823, 1.0, -2.180, 0.000, 0.000, 0.000, 0.980, 0.006, '  5 MC
'Fe 1',      6292.8215,  5.3411, 1.0, -2.493, 8.180,-4.710,-7.470, 2.100, 0.007, '  1 K14
'V 1',       6292.8244,  0.2866, 1.0, -1.490, 6.500,-6.160,-7.742, 1.600, 0.150, '  6 LWDFSC
'Si 1',      6293.3008,  6.0827, 1.0, -2.130, 9.160,-3.050,-7.250, 1.520, 0.026, '  4 K07
'Fe 1',      6293.6103,  5.0638, 1.0, -1.193, 8.800,-4.180,-7.340, 1.280, 0.170, '  1 K14
'Fe 2',      6293.7874,  3.2673, 1.0, -5.189, 8.540,-6.520,-7.900, 0.100, 0.009, '  9 K13
'Fe 1',      6293.9237,  4.8349, 1.0, -1.717, 8.300,-4.990,-7.420, 1.940, 0.101, '  1 K14
'Ti 1',      6295.2478,  0.0480, 1.0, -4.242, 5.130,-6.110,-7.770, 1.250, 0.007, '  11 K10
'Ti 1',      6295.9441,  1.7393, 1.0, -2.470, 8.220,-6.050,-7.700, 1.660, 0.007, '  12 LGWSC
'La 2',      6296.0790,  1.2516, 1.0, -0.950, 0.000, 0.000, 0.000, 1.120, 0.015, '  5 CB
'Fe 1',      6296.1799,  5.0638, 1.0, -1.967, 8.790,-4.070,-7.310, 0.780, 0.039, '  1 K14
'V 1',       6296.4909,  0.3006, 1.0, -1.610, 6.470,-6.160,-7.740, 1.550, 0.117, '  6 LWDFSC
'Ti 1',      6296.6459,  0.0000, 1.0, -3.582, 5.130,-6.110,-7.770, 0.530, 0.030, '  11 K10
'Ti 1',      6296.8525,  3.1390, 1.0, -1.131, 8.210,-5.070,-7.540, 0.760, 0.007, '  11 K10
'Co 1',      6296.9481,  2.0802, 1.0, -3.136, 8.120,-6.160,-7.800, 1.330, 0.010, '  13 K08
'Fe 1',      6297.7922,  2.2227, 1.0, -2.740, 8.290,-6.160,-7.694, 0.990, 0.565, '  1 K14
'Si 1',      6297.8890,  5.8708, 1.0, -2.919, 7.900,-3.400,-6.870, 1.100, 0.008, '  4 K07
'Ti 1',      6298.0732,  1.7335, 1.0, -2.440, 8.230,-5.980,-7.690, 1.980, 0.008, '  12 LGWSC
'Nd 2',      6298.4100,  0.9329, 1.0, -1.430, 0.000, 0.000, 0.000, 0.660, 0.006, '  15 HLSC
'Fe 1',      6298.4580,  4.6520, 1.0, -3.025, 8.320,-4.690,-7.510, 2.020, 0.010, '  1 K14
'Ni 1',      6298.7446,  5.2884, 1.0, -1.517, 8.420,-4.380,-7.490, 1.110, 0.009, '  16 K08
'Ce 2',      6299.4820,  1.8947, 1.0, -0.435, 0.000, 0.000, 0.000, 1.190, 0.005, '  17 PQWB
'Si 1',      6299.5987,  5.9840, 1.0, -1.335, 7.330,-2.530,-6.790, 1.130, 0.086, '  4 K07
'O 1',       6300.3038,  0.0000, 1.0, -9.819,-2.170, 0.000, 0.000,99.000, 0.005, '  2 WSG
'Ni 1',      6300.3350,  4.2661, 1.0, -2.275, 8.270,-5.400,-7.750, 0.510, 0.006, '  16 K08
```

```
'Ni 1',      6300.3550,  4.2661, 1.0, -2.695, 8.270,-5.400,-7.750, 0.510, 0.006, '  16 K08
'Sc 2',      6300.6977,  1.5070, 1.0, -1.898, 8.380,-6.590,-7.830, 1.320, 0.075, '  18 K09
'Fe 1',      6301.4995,  3.6537, 1.0, -0.718, 8.080,-5.410,-7.540, 1.670, 0.623, '  1 K14
'Si 1',      6301.6247,  5.9537, 1.0, -2.653, 7.470,-2.590,-6.810, 0.820, 0.011, '  4 K07
'Fe 1',      6302.4931,  3.6864, 1.0, -0.968, 8.080,-5.390,-7.540, 2.490, 0.581, '  1 K14
'Fe 1',      6303.4600,  4.3201, 1.0, -2.660, 8.380,-4.940,-7.277, 1.260, 0.042, '  14 FMW
'Si 1',      6303.6062,  6.0827, 1.0, -1.213, 9.040,-2.710,-6.990, 1.030, 0.153, '  4 K07
'Ti 1',      6303.7565,  1.4432, 1.0, -1.580, 8.260,-5.980,-7.585, 0.920, 0.089, '  12 LGWSC
'V 1',       6304.2617,  3.2863, 1.0,  0.199, 8.350,-4.900,-7.530, 1.270, 0.009, '  7 K09
'Zr 1',      6304.3400,  1.6294, 1.0,  0.000, 0.000, 0.000, 0.000,99.000, 0.009, '  19 MULT
'Fe 1',      6304.7893,  4.9913, 1.0, -0.864, 8.800,-4.410,-7.350, 1.390, 0.292, '  1 K14
'Mn 1',      6304.9289,  4.8889, 1.0, -0.532, 8.020,-3.820,-7.120, 1.970, 0.027, '  20 K07
'Fe 2',      6305.2955,  6.2187, 1.0, -2.094, 8.600,-6.530,-7.870, 1.290, 0.019, '  9 K13
'La 2',      6305.4470,  0.2443, 1.0, -2.380, 0.000, 0.000, 0.000, 1.050, 0.006, '  5 CB
'Sc 1',      6305.6570,  0.0209, 1.0, -1.240, 6.470,-6.110,-7.749, 1.200, 0.094, '  21 LD
'Mn 1',      6306.3646,  4.8889, 1.0, -0.656, 8.020,-3.760,-7.120, 1.640, 0.021, '  20 K07
'Cr 1',      6307.2698,  3.8904, 1.0, -1.645, 7.900,-6.000,-7.730, 1.110, 0.010, '  23 K10
'Fe 2',      6307.5201,  2.8281, 1.0, -5.566, 8.470,-6.530,-7.910, 1.400, 0.011, '  9 K13
'Fe 1',      6307.8540,  3.6416, 1.0, -4.325, 7.780,-6.220,-7.800, 1.340, 0.006, '  1 K14
'Si 1',      6308.8253,  5.8625, 1.0, -1.795, 7.380,-3.560,-6.920, 1.060, 0.082, '  4 K07
'V 1',       6309.7168,  2.5749, 1.0, -0.675, 7.480,-5.980,-7.770, 1.340, 0.007, '  7 K09
'Sc 2',      6309.9199,  1.4970, 1.0, -1.618, 8.380,-6.580,-7.830, 0.510, 0.133, '  18 K09
```

Bibliography

Allende Prieto, C., Lambert, D. L., & Asplund, M. 2001, ApJ, 556, L63

Alothman, A. 2016, emaze Milky Way Galaxy

Amarsi, A. M., Lind, K., Asplund, M., Barklem, P. S., & Collet, R. 2016, MNRAS, 463, 1518

Bensby, T. 2004, Introduction (Lund, Sweden: Lund University Observatory), 1–9

Bensby, T., Feltzing, S., & Lundström, I. 2003, in Astronomical Society of the Pacific Conference Series, Vol. 304, CNO in the Universe, ed. C. Charbonnel, D. Schaerer, & G. Meynet, 175

Bensby, T., Feltzing, S., & Lundström, I. 2004, A&A, 415, 155

Bensby, T., Feltzing, S., & Oey, M. S. 2014, A&A, 562, A71

Bertran de Lis, S., Delgado Mena, E., Adibekyan, V. Z., Santos, N. C., & Sousa, S. G. 2015, A&A, 576, A89

Gustafsson, B., Edvardsson, B., Eriksson, K., et al. 2008, A&A, 486, 951

Haywood, M. 2012, in European Physical Journal Web of Conferences, Vol. 19, European Physical Journal Web of Conferences, 05001

Matteucci, F. 2012, Introduction (Berlin, Heidelberg: Springer Berlin Heidelberg), 2–3

McWilliam, A. 1997, ARA&A, 35, 503

Ramírez, I., Allende Prieto, C., & Lambert, D. L. 2013, ApJ, 764, 78

Sneden, C., Lambert, D. L., & Whitaker, R. W. 1979, ApJ, 234, 964

Tinsley, B. M. 1979, ApJ, 229, 1046

Wikipedia. 2017, Wikipedia Milky Way Galaxy edge-on structure